Laser-Induced Spatiotemporal Dynamics of Magnetic Films

Ka Shen[1] and Gerrit E. W. Bauer[2,1]

[1]*Kavli Institute of NanoScience, Delft University of Technology, Lorentzweg 1, 2628 CJ Delft, The Netherlands*
[2]*Institute for Materials Research and WPI-AIMR, Tohoku University, Sendai 980-8577, Japan*

We present a theory for the coherent magnetization dynamics induced by a focused ultrafast laser beam in magnetic films, taking into account nonthermal (inverse Faraday effect) and thermal (heating) actuation. The dynamic conversion between spin waves and phonons is induced by the magnetoelastic coupling that allows efficient propagation of angular momentum. The anisotropy of the magnetoelastic coupling renders characteristic angle dependences of the magnetization propagation that are strikingly different for thermal and nonthermal actuation.

Introduction.—Since the discovery of laser-induced ultrafast spin dynamics in nickel by Beaurepaire *et al.* [1], the spin manipulation in a ferromagnetic system by femtosecond laser pulses has attracted much attention since combining the intellectual challenge of new physics with the application of the potential of ultrafast magnetization reversal [2]. Intense light can cause many effects in magnets, such as the coherent inverse Faraday effect (IFE) as well as the excitation of the coupled electron, magnon, and phonon subsystems on various time scales. The associated modulation of the magnetic anisotropy and magnetization modulus allows coherent control of the magnetic order [3,4]. The transient magnetic field generated by the IFE allows nonthermal ultrafast magnetization control [5,6] that may be distinguished from heating-induced effects by switching the light polarization. Nevertheless, heating is essential for light-induced magnetization reversal [7]. Toggle switching of the magnetization by heat alone has also been reported [8]. Understanding and controlling the relative magnitude of thermal and nonthermal excitation is therefore an important but unsolved issue.

The optical ultrafast pump-probe technique as shown in Fig. 1 is an established powerful method to study matter. Here we will show that the symmetry of the spatiotemporal magnetization distribution excited by a focused laser beam reveals the relative contributions of thermal and nonthermal excitations. This phenomenon originates from the magnetoelastic coupling (MEC) [9–11], i.e., the coupling between spin waves (magnons) and acoustic lattice waves (phonons).

In the regions of phase space in which the magnon and phonon dispersion come close, the MEC hybridizes magnons and phonons into coherently mixed quasiparticles ["magnon polarons"(MPs)]. This implies that phonons in magnets can be converted into magnetization and become detectable via magneto-optical [12–14] or electrical [15,16] techniques. In this Letter, we present a study of the spatial magnetization dynamics in magnetic thin films after focused-laser excitation [17]. We consider here magnetic insulators that are not affected by conduction or

photoexcited free carriers. We find that laser-generated phonons efficiently excite magnetization when the diameter of the laser spot is comparable with the wavelength of the MPs. The spatial dynamics of such phonon-induced magnetization shows a different angular symmetry from that of the magnetization generated directly by laser via the IFE. Dedicated experiments suggested here can therefore help understanding the fundamental nature of light-matter interaction in magnets.

Formalism.—The basic theory for MPs in special symmetry directions by Kittel [9] and Akhiezer *et al.* [10], extended by Schlömann [11] to arbitrary propagating directions, was developed more than half a century ago. The energy density of the minimal model reads [9]

$$\mathcal{H} = \mathcal{H}_{ex} + \mathcal{H}_Z + \mathcal{H}_{el} + \mathcal{H}_{mec} + \mathcal{H}_{dip}. \tag{1}$$

We adopt a cubic unit cell and consider the thin film limit in which the magnetization is spatially constant over the film thickness. This assumption holds for films up to 100 μm [17], which for wide-gap insulators is still less than the penetration depth of the light and allows us to use a two-dimensional model. With external magnetic field $\mathbf{H}$ and equilibrium magnetization vector $\mathbf{M}_0 \| \mathbf{x}$ ($|\mathbf{M}_0| = M_0$
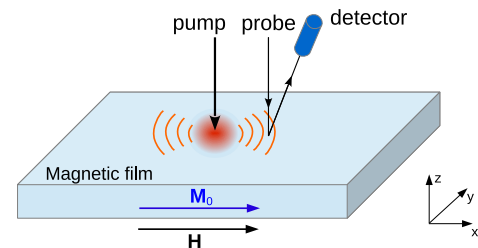

FIG. 1 (color online). Pump-probe study of the dynamics of magnetic films by pulsed lasers: An external magnetic field aligns the equilibrium magnetization along the x direction. The pump laser hits the sample at the origin in time and space. The temporal distribution of the out-of-plane (z) component of the magnetization is detected by the Kerr rotation of the linearly polarized probe pulse.

saturation magnetization) $\mathcal{H}_{ex} = A[(\nabla m_y)^2 + (\nabla m_z)^2]$ and $\mathcal{H}_Z = -\mu_0 H M_0 + (\mu_0 H M_0/2)(m_y^2 + m_z^2)$ represent the (linearized) exchange and Zeeman energies, respectively, where m_y and m_z are the transverse magnetization components of $\mathbf{m} = \mathbf{M}/M_0$. $\mathcal{H}_{el}$ is the lattice energy with both kinetic and elastic contributions $\mathcal{H}_{el} = (1/2)\rho \dot{\mathbf{R}} \cdot \dot{\mathbf{R}} + (1/2)\lambda(\sum_i S_{ii})^2 + \mu \sum_{ij} S_{ij}^2$ with strain tensor $S_{ij} = (\partial_i R_j + \partial_j R_i)/2$ and $\mathbf{R}$ representing the lattice displacement with respect to equilibrium, ρ the mass density, and λ and μ elastic constants. The MEC in Eq. (1) reads $\mathcal{H}_{mec} = \sum_{i,j \in \{y,z\}}(b + a\delta_{ij})S_{ij}m_i m_j + 2b\sum_{i \in \{y,z\}}S_{ix}m_i$, where a and b are magnetoelastic coupling coefficients. By adopting the short-wave length limit of the magnetostatic dipolar interaction $\mathcal{H}_{dip} \approx (\mu_0 M_0^2/2)m_y^2 \sin^2 \theta$, we disregard the Damon-Eshbach surface modes [18] and simplify the dispersion of the volume modes, which is allowed for small laser spot sizes with response being dominated by high-momentum wave vectors [19].

By introducing the forces and torques $\mathbf{F}$ acting on the displacement vector $\Phi = (m_y, m_z, R_l, R_t, R_z)^T$, one can write out the linearized equations of motion as shown in the Supplemental Material [20]. Here, the lattice displacement is rewritten in the form of longitudinal (R_l), in-plane transverse (R_t), and out-of-plane transverse (R_z) modes. Strictly speaking, the damping of phonons and magnons are not necessarily independent, since magnetization is affected by phonon attenuation via the MEC [27]. We treat the Gilbert damping constant α and phonon relaxation time τ_p as independent parameters since Gilbert damping can also be caused by magnetic disorder, surface roughness, or defects [28]. We define the anisotropic spin wave frequency $\Omega_0 = \gamma\mu_0\sqrt{H(H + M_0 \sin^2 \theta)}$ and the MEC frequency parameter $\Delta(k) = \sqrt{\gamma b^2 k^2/(4M_0 \rho \Omega_0)}$ with θ being the angle between the magnetic field and in-plane wave vector $\mathbf{k}$.

The spatiotemporal dynamics of $\Phi(\mathbf{r}, t)$ reads

$$\Phi_i(\mathbf{r}, t) = \int d\mathbf{r}' dt' G_{ij}(\mathbf{r} - \mathbf{r}', t - t')F_j(\mathbf{r}', t'), \quad (2)$$

where G_{ij} are the components of the Green function matrix (propagator) associated with the magnetoelastic equations of motion specified in the Supplemental Material [20]. A femtosecond laser pulse generates forces via the inverse Faraday effect [2,17,29] and heating [14,30–32] that are instantaneous on the scale of the lattice and magnetization dynamics. The relative importance of these two mechanisms depends on the material and light and is still a matter of controversy. Here we find that spot excitation of thin magnetic films is an appropriate method to separate the two, since they lead to conspicuous differences in the time and position dependent response.

We consider circularly polarized light along z that by the IFE generates an effective magnetic field along the same direction. For a femtosecond Gaussian pulse with spot size W, the generated magnetic field has a spatial distribution

$\mathbf{H}_{IFE}(\mathbf{r}, t) = \hat{z}H_{IFE}f(t)\exp(-r^2/W^2)$, where temporal shape $f(t) \approx \tau_l \delta(t)$ with pulse duration τ_l; the amplitude $H_{IFE} = \beta I_{in}\sigma$ is proportional to laser intensity (I_{in}) and IFE coefficient (β), respectively. The latter is related to the Verdet constant (V) as $\beta = V\lambda_0/(2\pi c_0)$, where λ_0 and c_0 are wavelength and velocity of the light [33]. $\sigma = 1(-1)$ for left(right)-handed polarization. The torque $F_{m_y}(\mathbf{r}, t) = \gamma\tau_l\mu_0 H_{IFE}\delta(t)\exp(-r^2/W^2)$. On the other hand, the light pulse generates a sudden increase of the local lattice temperature $\delta T(\mathbf{r}, t) = [\Gamma I_{in}\tau_l/(\rho C_v)]\Theta(t)\exp(-r^2/W^2)$, where Γ is the light-absorption coefficient. By choosing the Heaviside step function $\Theta(t)$, we assume that the lattice locally equilibrates much faster than the response time of the coherent magnetization (a few picoseconds [34]), while the subseqent cooling of the lattice by diffusion is slow. The resulting in-plane thermoelastic stress $F_{R_l} = \eta(3\lambda + 2\mu)\partial_r T$ generates longitudinal (pressure) waves [31,35], where η is the thermoelastic expansion coefficient. The local thermal expansion also generates a "bulge" shear stress [36] at a free surface, i.e., an out-of-plane displacement R_z. $F_{R_z} = \zeta\eta\nabla^2 T$, where ζ is a parameter proportional to the film thickness and controlled by the substrate and an eventual cap layer, leads to displacement proportional to the local temperature gradient (see numerical results below). In the Supplemental Material [20], we specify the material parameters for yttrium iron garnet (YIG) adopted in our calculations.

One-dimensional dynamics.—We start with a spin wave propagating along the external magnetic field, i.e., $\theta = 0$, which by symmetry couples only with the transverse phonons. The IFE generates the torque $F_{m_y}(x, t) = m_0\delta(t)\exp(-x^2/W^2)$ with $m_0 = \gamma\tau_l\mu_0 H_{IFE}$. This can be realized by a line-shaped excitation spot [17].

The calculated magnetization profiles at $\Omega_0 t = 50$ and 75 without and with MEC are plotted in Figs. 2(a) and 2(b) separately for $\alpha = 10^{-4}$. Without MEC the magnetization is localized at the exposure spot and broadens only very weakly with time, while the MEC strongly enhances the broadening of the primary magnetization packet, with a wave front propagating with the sound velocity c_t. This phenomenon illustrates that the lattice plays an essential role for spin transport in magnetic films.

Figure 2(c) illustrates the sound-assisted propagation for Gilbert damping $\alpha = 0.1$. Instead of the expanding wave front in Fig. 2(b), we now find two packets escaping the excitation region into opposite directions. The packets have a much longer lifetime than the coherently generated IFE magnetization and, hence, dominate at long time scales. This behavior is recovered by the asymptotic expression obtained when $\alpha \gg \tilde{\Delta}(\tilde{k}_c)$ at the magnon-phonon dispersion crossing wave vector ($\tilde{k}_c = 1/\tilde{c}_t$),

$$m_z(\tilde{x}, \tilde{t}) \simeq m_0 e^{-\alpha\tilde{t}-\tilde{x}^2}\sin(\tilde{t}) + (2\alpha)^{-1}m_0 e^{-\tilde{t}/\tilde{\tau}_p}\tilde{\Delta}^2(\tilde{k}_c)$$
$$\times \begin{cases} 2\alpha\tilde{c}_t^2[\Lambda_1(\tilde{c}_t\tilde{t} - \tilde{x}) + \Lambda_1(\tilde{c}_t\tilde{t} + \tilde{x})], & \tilde{c}_t \ll 1, \\ \tilde{c}_t^{-1}\sqrt{\pi}[\Lambda_2(\tilde{c}_t\tilde{t} - \tilde{x}) + \Lambda_2(\tilde{c}_t\tilde{t} + \tilde{x})], & \tilde{c}_t \geq 1, \end{cases}$$
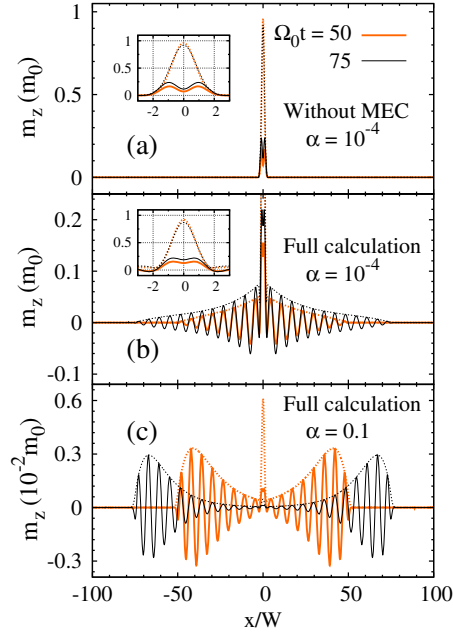$$(3)$$

FIG. 2 (color online). One-dimensional model for the dynamics of the out-of-plane magnetization component m_z induced by the inverse Faraday effect: (a) At times $\Omega_0 t = 50$ and 75 for a Gaussian laser intensity spot in the absence of MEC with Gilbert damping $\alpha = 10^{-4}$. The dashed envelopes are the modulus ($|\mathbf{m} - \hat{x}|$). (b) With $\alpha = 10^{-4}$ and (c) with $\alpha = 0.1$ are computed for MEC parameter $\tilde{\Delta}(\tilde{k}_c) = 0.02$. Common are the exchange parameter $\tilde{D} = 0.02$, sound velocity $\tilde{c}_t = 1$, and sound attenuation rate $\tilde{\tau}_p^{-1} = 10^{-3}$. Note the change of scale between (b) and (c). The insets provide an expanded view of the laser spot.

where $\Lambda_1(\xi) = (1/\sqrt{\pi}) \int_0^\infty d\tilde{k}\tilde{k}^2 \sin(\tilde{k}\xi) \exp(-\tilde{k}^2/4)$ and $\Lambda_2(\xi) = \exp[-(\xi^2\alpha^2 + 1)/(2\tilde{c}_t)^2] \sin(\xi/\tilde{c}_t)$ and W and Ω_0 have been by rendered dimensionless as explained in the Supplemental Material [20]. The (purely magnetic) first term on the right-hand side represents the exponential decay of the initially excited wave packet, while the second term is a propagating MP mode. The latter is damped only by the lattice and hence, may have a very long mean free path for materials with high acoustic quality like YIG (assuming that doping affects the magnetization without increasing sound attenuation).

When the laser spot size is large relative to the MP wavelength, i.e., $\tilde{c}_t \ll 1$, according to Eq. (3) the ratio between MP amplitude and IFE strength scales as $\tilde{c}_t^2 \tilde{\Delta}^2(\tilde{k}_c)$, i.e., increases with sound velocity and decreases with spot size. In the other limit, $\tilde{c}_t \gg 1$, the amplitude of the long-lived signal is inversely proportional to $\tilde{c}_t$, therefore, it decreases with increasing $\tilde{c}_t$. We therefore estimate this ratio to be maximal $e^{-1/4}\sqrt{\pi}\tilde{\Delta}^2(\tilde{k}_c)/(2\alpha)$ when the laser spot size matches the MP wavelength. The peak amplitude of MPs in Fig. 2(c) is around 3×10^{-3}, in good agreement with $e^{-1/4}\sqrt{\pi}\tilde{\Delta}^2(\tilde{k}_c)/(2\alpha) \approx 2.7 \times 10^{-3}$.

Thermal actuation is caused by the shear force generated by the laser heating profile $F_{R_z}(x,t) = (\zeta\eta c_t^2\Gamma I_{\text{in}}\tau_l/C_v)\Theta(t)\partial_x^2 \exp(-x^2/W^2)$, since the pressure wave is decoupled

from the spin wave at $\theta = 0$. The asymptotic expression for $\alpha \gg \tilde{\Delta}(\tilde{k}_c)$ becomes

$$m_z(x,t) = m_1$$
$$\times \begin{cases} \tilde{c}_t\{\Lambda_3(\tilde{x}) - (1/2)e^{-\tilde{t}/\tilde{\tau}_p} \\ \quad \times[\Lambda_3(\tilde{c}_t\tilde{t}+\tilde{x}) - \Lambda_3(\tilde{c}_t\tilde{t}-\tilde{x})]\} \quad , \quad \tilde{c}_t \ll 1, \\ \tilde{c}_t(1 - e^{-\alpha t}\cos t)\Lambda_3(\tilde{x}) + \tilde{c}_t^{-1}(\sqrt{\pi}/4) \\ \quad \times e^{-\tilde{t}/\tilde{\tau}_p}[\Lambda_4(\tilde{c}_t\tilde{t}+\tilde{x}) - \Lambda_4(\tilde{c}_t\tilde{t}-\tilde{x})] \quad , \quad \tilde{c}_t \geq 1, \end{cases}$$
(4)

where $\Lambda_3(\xi) = \xi\exp(-\xi^2)$ and $\Lambda_4(\xi) = \exp[-(\xi^2\alpha^2 + 1)/(2\tilde{c}_t)^2]\cos(\xi/\tilde{c}_t)$. For YIG, the parameter $m_1 = \gamma b\zeta\eta\Gamma I_{\text{in}}\tau_l/(2M_0\rho c_t C_v) \sim 10^3\zeta\delta T\,\text{m}^{-1}\,\text{K}^{-1}$. Compared to Eq. (3), the heat-induced magnetization has (i) odd parity in real space, i.e., $m_z(-x,t) = -m_z(x,t)$, (ii) a long-lived localized signal near the excitation spot, and (iii) maximum amplitude of propagation at $\tilde{c}_t \simeq 1$; cf. Fig. 3. We also plot the amplitude of the thermally generated phonon wave front that is trailed by the magnetization.

Two dimensions.—In the following, magnetization is oriented along $\hat{x}$ by an external in-plane magnetic field $\mu_0 H = 50$ mT corresponding to $\gamma\mu_0 H/(2\pi) \simeq 1.4$ GHz. The spot size $W = 1\ \mu$m and the dimensionless velocities are $\tilde{c}_t \approx 0.43$ and $\tilde{c}_l \approx 0.82$. Figure 4 summarizes our main results for the IFE and heat induced dynamics in terms of the out-of-plane magnetization component m_z. We plot a snapshot at $t = 5$ ns in the x-y (film) plane from the calculation with low ($\alpha = 10^{-4}$) and enhanced ($\alpha = 0.1$) magnetic damping in (a) and (b), respectively. Figure 4(a), left, displays IFE actuated outgoing rays that broaden with distance from the excitation spot. This feature is insensitive to MEC strength and can be understood by the angular dependent group velocities of magnetostatic spin wave dispersion around the average modulus of the wave vectors k_0. As discussed in the Supplemental Material [20], the group velocity $\mathbf{v}_g \simeq \hat{\theta}[\gamma\mu_0 M_0/(2k_0)]\sin 2\theta\sqrt{H/(H + M_0\sin^2\theta)}$ generates an expansion of the initial wave packet as shown by
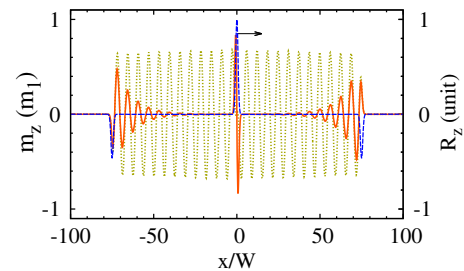

FIG. 3 (color online). Out-of-plane magnetization dynamics m_z with Gilbert damping $\alpha = 10^{-4}$ (dotted curve) and 0.1 (solid curve) induced by the spot heating by a laser pulse. The blue dashed curve shows the displacement profile (R_z). Other parameters are those in Fig. 2.
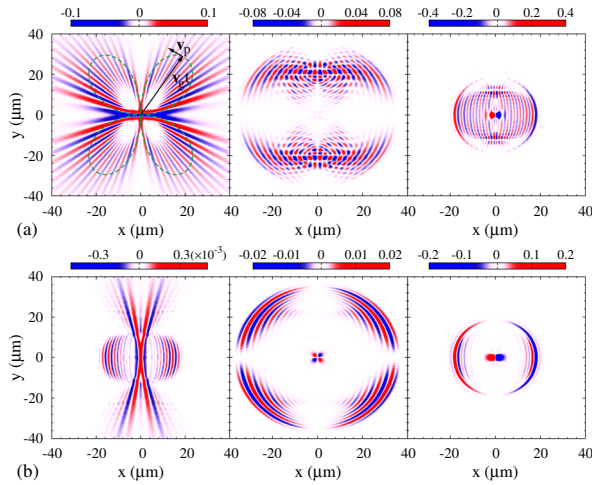
FIG. 4 (color online).   Two dimensional profile of out-of-plane magnetization m_z at $t = 5$ ns due to (left) IFE field F_{m_y}, (middle) pressure stress F_{R_l}, and (right) shear stress F_{R_z}. We normalize the result by m_0 for (left), $m_2 = \gamma b \eta \Gamma I_{in} \tau_l (3\lambda + 2\mu)/(2M_0 \rho^2 C_v c_t^2 \Omega_0)$ for (middle), and m_1 for (right). The Gilbert damping coefficient $\alpha = 10^{-4}$ and 0.1 for (a) and (b), respectively. The dashed (olive) curve in (a), left, illustrates the angular-dependent spin wave group velocity.

the dashed (olive) curve, while the the starlike interference fringes are governed by the phase velocity. At larger magnetic damping, cf. Fig. 4(b), left, the starlike features in the $\hat{x}$ direction are suppressed in favor of MP propagation with transverse sound velocity c_t. The dotted features around $c_l t$ are caused by interference of the longitudinal MP and the damped residue of the initial magnetization wave packet with $\theta \simeq 0$, which has relative longer lifetime. Note the mirror symmetry with respect to the y axis, $m_z(x, y) = m_z(-x, y)$.

The quadrupolar features in Fig. 4 (middle) with nodes along the x and y axes and $\sin 2\theta$ symmetry, are induced by the pressure F_{R_l} caused by a heat pulse. The radii of the circular wave fronts correspond to the longitudinal sound velocity. Figure 4, right, illustrates that a shear stress induces MPs that spread with transverse sound velocity c_t, which are thereby clearly distinguishable from the pressure induced signals: F_{R_z} generates dipolar symmetric features with nodes at the y axis, which follows from the $\cos \theta$ symmetry of the MEC coupling. Clearly, both heat-induced signals are antisymmetric with respect to reflection at the y axis, $m_z(x, y) = -m_z(-x, y)$, which allows discrimination from the IFE response. Moreover, we identify a nonpropagating signal in the vicinity of the excitation spot [see the center of Fig. 4(b), middle and right], a "smoking gun" for thermally excited dynamics.

It is not easy to predict the absolute and relative magnitude of the two mechanisms for a given light intensity from first principles due to uncertainties in the strongly nonequilibrium processes after an intense fs light pulse. Microscopic theories address the ultrafast physics of angular momentum and energy transfer from the light to the

magnetic order [37,38] and the lattice [34] and should ideally be employed to fix the initial conditions for our calculations. But also the long-time response depends on several temperature and frequency dependent materials' parameters that govern the IFE, light absorption, etc. Satoh *et al.* [17] find a Faraday rotation of the probe pulse of the order of a millirad for 110 μm thick bismuth-doped iron garnet, which corresponds to a light-induced torque of $m_0 \sim 0.004$ for a Verdet constant of 10^4 rad m^{-1} T^{-1} [20]. With thermal expansion coefficient $\eta \sim 10^{-5}$/K [39], the thermal torque $m_2 \sim 4 \times 10^{-3} \delta T$/K, which can be larger than m_0 for pulsed laser-induced heating [40]. Similar values may be anticipated for m_1 when effective thicknesses $\zeta \sim \mu$m. We should also not forget that the fast light-induced demagnetization [1] should affect the response directly under the excitation spot, but its diffusion should be slower than the ballistic response computed here.

Conclusion and discussion.—We modeled the spatio-temporal laser-induced magnetization dynamics in magnetic thin films, concluding that magnetoelastic coupling is essential for spin angular momentum transport because the phonon group velocity is much larger than that of the magnons. An experimental study of the symmetry of time-resolved magnetization wave fronts radiating from the excitation spot allows discriminating different laser excitation mechanisms, thereby helping to answer the long-standing question on the physical origin of ultrafast magnetization dynamics, i.e., whether it is caused by coherent light-induced magnetic fields or sudden heating of the lattice. Moreover, we clarified the optimal size of the excitation laser spot to be the MP wavelength; for YIG at an applied field of 50 mT it is ~1 μm.

The essential role of the MEC coupling might have larger ramifications. For example, a number of recent experiments on the spin Seebeck effect on YIG came to the conclusion that the thermal spin pumping is not caused by terhahertz magnons at energies around $k_B T$, but by spin waves in a low energy band close to the gap [41–43]. Spin information was found to propagate in YIG diffusely over large distances [44,45]. From the present results we venture that strongly coupled magnon-polarons could be the carriers of thermal spin currents.

Note added—.Ogawa *et al.* report generation of laser-generated magnon polarons that drive magnetic bubble domains [46].

[1] E. Beaurepaire, J.-C. Merle, A. Daunois, and J.-Y. Bigot, Phys. Rev. Lett. **76**, 4250 (1996).

[2] A. Kirilyuk, A. V. Kimel, and T. Rasing, Rev. Mod. Phys. **82**, 2731 (2010).

[3] G. Ju, A. V. Nurmikko, R. F. C. Farrow, R. F. Marks, M. J. Carey, and B. A. Gurney, Phys. Rev. Lett. **82**, 3705 (1999).

[4] M. van Kampen, C. Jozsa, J. T. Kohlhepp, P. LeClair, L. Lagae, W. J. M. de Jonge, and B. Koopmans, Phys. Rev. Lett. **88**, 227201 (2002).

[5] A. V. Kimel, A. Kirilyuk, P. A. Usachev, R. V. Pisarev, A. M. Balbashov, and T. Rasing, Nature (London) **435**, 655 (2005).

[6] F. Hansteen, A. Kimel, A. Kirilyuk, and T. Rasing, Phys. Rev. Lett. **95**, 047402 (2005).

[7] K. Vahaplar, A. M. Kalashnikova, A. V. Kimel, D. Hinzke, U. Nowak, R. Chantrell, A. Tsukamoto, A. Itoh, A. Kirilyuk, and T. Rasing, Phys. Rev. Lett. **103**, 117201 (2009).

[8] J. Barker, U. Atxitia, T. A. Ostler, O. Hovorka, O. Chubykalo-Fesenko, and R. W. Chantrell, Sci. Rep. **3**, 3262 (2013).

[9] C. Kittel, Phys. Rev. **110**, 836 (1958).

[10] A. I. Akhiezer, V. G. Bar'yakhtar, and S. V. Peletminskii, Zh. Eksp. Teor. Fiz. **35**, 228 (1958).

[11] E. Schlömann, J. Appl. Phys. **31**, 1647 (1960).

[12] A. V. Scherbakov, A. S. Salasyuk, A. V. Akimov, X. Liu, M. Bombeck, C. Brüggemann, D. R. Yakovlev, V. F. Sapega, J. K. Furdyna, and M. Bayer, Phys. Rev. Lett. **105**, 117204 (2010).

[13] J.-W. Kim, M. Vomir, and J.-Y. Bigot, Phys. Rev. Lett. **109**, 166601 (2012).

[14] J. V. Jäger, A. V. Scherbakov, B. A. Glavin, A. S. Salasyuk, R. P. Campion, A. W. Rushforth, D. R. Yakovlev, A. V. Akimov, and M. Bayer, arXiv:1505.01729.

[15] K. Uchida, H. Adachi, T. An, T. Ota, M. Toda, B. Hillebrands, S. Maekawa, and E. Saitoh, Nat. Mater. **10**, 737 (2011).

[16] M. Weiler, H. Huebl, F. S. Goerg, F. D. Czeschka, R. Gross, and S. T. B. Goennenwein, Phys. Rev. Lett. **108**, 176601 (2012).

[17] T. Satoh, Y. Terui, R. Moriya, B. A. Ivanov, K. Ando, E. Saitoh, T. Shimura, and K. Kuroda, Nat. Photonics **6**, 662 (2012).

[18] R. W. Damon and J. R. Eshbach, J. Phys. Chem. Solids **19**, 308 (1961).

[19] A. A. Serga, P. Clausen, A. V. Chumak, and B. Hillebrands, Annual Report 2012, http://www.physik.uni-kl.de/hillebrands/publications/annual-reports/annual-report-2012.

[20] See Supplemental Material at http://link.aps.org/supplemental/10.1103/PhysRevLett.115.197201 contains technical discussions with reference to [21–26].

[21] S. A. Manuilov, S. I. Khartsev, and A. M. Grishin, J. Appl. Phys. **106**, 123917 (2009).

[22] A. G. Gurevich and G. A. Melkov, *Magnetization Oscillations and Waves* (CRC Press, Boca Raton, 1996).

[23] A. A. Serga, A. V. Chumak, and B. Hillebrands, J. Phys. D **43**, 264002 (2010).

[24] M. A. Gilleo and S. Geller, Phys. Rev. **110**, 73 (1958).

[25] M. F. Lewis and E. Patterson, J. Appl. Phys. **39**, 1932 (1968).

[26] J. G. Bai, G.-Q. Lu, and T. Lin, Sensors and Actuators A: Physical **109**, 9 (2003).

[27] C. Vittoria, S. D. Yoon, and A. Widom, Phys. Rev. B **81**, 014412 (2010).

[28] G. G. Siu, C. M. Lee, and Y. Liu, Phys. Rev. B **64**, 094421 (2001).

[29] A. H. M. Reid, A. V. Kimel, A. Kirilyuk, J. F. Gregg, and T. Rasing, Phys. Rev. B **81**, 104404 (2010).

[30] O. B. Wright and K. Kawashima, Phys. Rev. Lett. **69**, 1668 (1992).

[31] C. Rossignol, J. M. Rampnoux, M. Perton, B. Audoin, and S. Dilhaire, Phys. Rev. Lett. **94**, 166106 (2005).

[32] H. Park, X. Wang, S. Nie, R. Clinite, and J. Cao, Phys. Rev. B **72**, 100301 (2005).

[33] P. S. Pershan, J. P. van der Ziel, and L. D. Malmstrom, Phys. Rev. **143**, 574 (1966).

[34] E. S. Zijlstra, A. Kalitsov, T. Zier, and M. E. Garcia, Phys. Rev. X **3**, 011005 (2013).

[35] S. J. Davies, C. Edwards, G. S. Taylor, and S. B. Palmer, J. Phys. D **26**, 329 (1993).

[36] R. J. Dewhurst, D. A. Hutchins, S. B. Palmer, and C. B. Scruby, J. Appl. Phys. **53**, 4064 (1982).

[37] G. Lefkidis, G. P. Zhang, and W. Hübner, Phys. Rev. Lett. **103**, 217401 (2009).

[38] U. Atxitia, O. Chubykalo-Fesenko, R. W. Chantrell, U. Nowak, and A. Rebei, Phys. Rev. Lett. **102**, 057203 (2009).

[39] T. Boudiar, B. Payet-Gervy, M.-F. Blanc-Mignon, J.-J. Rousseau, M. L. Berre, and H. Joisten, J. Magn. Magn. Mater. **284**, 77 (2004).

[40] G.-M. Choi, C.-H. Moon, B.-C. Min, K.-J. Lee, and D. G. Cahill, Nat. Phys. **11**, 576 (2015).

[41] T. Kikkawa, K.-i. Uchida, S. Daimon, Z. Qiu, Y. Shiomi, and E. Saitoh, Phys. Rev. B **92**, 064413 (2015).

[42] H. Jin, S. R. Boona, Z. Yang, R. C. Myers, and J. P. Heremans, Phys. Rev. B **92**, 054436 (2015).

[43] E. Guo, A. Kehlberger, J. Cramer, G. Jakob, and M. Kläui, arXiv:1506.06037.

[44] L. J. Cornelissen, J. Liu, R. A. Duine, J. Ben Youssef, and B. J. van Wees, Nat. Phys. (to be published).

[45] B. L. Giles, Z. Yang, J. Jamison, and R. C. Myers, arXiv:1504.02808.

[46] N. Ogawa, W. Koshibae, A. J. Beekman, N. Nagaosa, M. Kubota, M. Kawasaki, and Y. Tokura, PNAS **112**, 8977 (2015).